Eur. Phys. J. D (2017) 71: 217
DOI: 10.1140/epjd/e2017-80238-y

THE EUROPEAN PHYSICAL JOURNAL D

Regular Article

Electron capture from H_2 molecule by He^+ ions

Hoda Ghavaminia[1,a], Laszlo Gulyas[2], Laszlo Sarkadi[2], Erika Bene[2], Sandor Demes[2], and Zoltan Juhasz[2]

[1] Physics Department, Dezful Branch, Islamic Azad University, Dezful, Iran
[2] Institute for Nuclear Research of the Hungarian Academy of Sciences (Atomki), P.O. Box 51, 4001 Debrecen, Hungary

Received 5 April 2017 / Received in final form 12 June 2017
Published online 29 August 2017 –

Abstract. The dynamics of the electron capture by He^+ ions from H_2 molecule has been investigated in the four-body first Born approximation. Cross sections differential in the scattering angle of the projectile ion have been calculated for various molecular orientations. The calculations account for the interference effects due to the coherent scattering of the particles from the two atomic centers. Total cross sections (integrated over the projectile's scattering angle and averaged over all the molecular orientations) have also been calculated by a three-body version of the classical trajectory Monte Carlo (CTMC) method based on use of a two-center molecular potential, as well as in a semi-classical quasi-molecular model. The obtained total cross sections are compared with the available experimental data and other theoretical calculations. For impact energies above 40 keV a reasonable agreement has been found between the present theoretical results and the experiment.

1 Introduction

In contrast to stationary phenomena, the theoretical description of the dynamics of many-body systems at the microscopic level faces large problems due to its complexity. One example of such a many-body dynamics is the scattering of charged ions on atomic or molecular targets, where various processes can take place. The incoming ion can ionize or excite the target or capture one or more electrons. The cross sections for these various processes depend on the properties of the target and the projectile as well as on the collision energy. Electron transfer processes have received considerable attention in various branches of physics and also in other sciences, as well as in technology and industry. Atomic collisions affect to a large extent the plasma radiation which is one of the plasma-cooling mechanisms in tokamacs. Furthermore, they also determine the transport of neutral particles and the flux distribution of the momentum and energy in the plasma [1].

Studies of ionization or electron capture processes for molecular species show up slower progresses than for atomic ones. Several problems emerge in the case of molecular targets. On the experimental side, it is not possible yet to prepare the molecular target in a particular rotational or vibrational state. Also, due to the different rotational and vibrational states of the molecules the theoretical descriptions of reactions are very demanding as in realistic descriptions of the processes the molecular structure must be fully included. Even for the simplest diatomic molecules such as H_2 the sophisticated wave functions eventuate the collisional problem almost unmanageable. Therefore, several approximations have been developed.

The H_2 target has received a lot of attention as it may serve as a test case involving most of the complications of the molecular targets. The oscillatory structure in differential cross sections due to the interference effect observed in collisions of ions with H_2 molecule [2] has a significance for several reasons. The coherent electron emission or scattering of the projectile ion from the H_2 molecule may be regarded as an analogy of the well-known Young's double slit experiment. Another important point is that the observed interference pattern sensitively depends on the collision dynamics. This explains the large number of investigations in the past 40 years dealing with interference effects in different collision processes involving the H_2 molecule (electron capture, photoionization, heavy-particle bombardment, etc.).

For the case of electron emission, either very simple descriptions, like plane waves [3,4] or somewhat complicated descriptions, employing approximate orthogonalized one-center Coulomb waves [5,6] were used in the past. As a recent development the triple differential cross section for the $(e, 2e)$ ionization of the diatomic hydrogen by fast electron impact was determined using two-effective center approximation [8]. Electron capture from hydrogen molecule by proton was treated using the second-order Born approximation [10]. The continuum distorted wave (CDW), the continuum distorted wave eikonal initial state (CDW-EIS) and the continuum distorted wave-eikonal final state (CDW-EFS) approximations were generalized for hydrogen molecular targets [13].

[a] e-mail: ghavaminia61@gmail.com

The single electron capture process in the collision of fast proton with ground-state hydrogen molecule was studied recently by applying a one active-electron model [14]. In the present work, we use the four-body first-order Born (B1) approximation, a three-body version of the classical trajectory Monte Carlo (CTMC) method, and a quasi-molecular model to evaluate the cross sections for the He^+-H_2 collisions in a broad range of the collision energy. The He^+ projectile is interesting from that point of view that the description of the collision processes with clothed ions brings additional difficulties in the theoretical treatment. The simplest way to represent the potential of a dressed projectile is the use of a constant effective nuclear charge provided, e.g. by the Slater's rule. In this case the projectile is still represented by a pure Coulomb field. A more realistic description can be given when a short range field due to the static screening of the electron(s) is added to the potential of the nucleus (see, e.g., Refs. [15,16]) for the treatment of atomic collisions. In the present work the field of the dressed projectile is approximated by an effective nuclear charge in B1, and by a screened potential in CTMC. In the quasi-molecular calculations such approximations were not needed, because all the three electrons were involved in the treatment of the molecular dynamics.

The structure of this paper is as follows. In Section 2.1 the differential cross section factorized into interference and atomic terms for the process of electron capture from the H_2 molecule by ion impact is derived in the B1 approximation. In Section 2.2 the CTMC theory for the description of molecular collisions is introduced. In Section 2.3 the quasi-molecular model is outlined. In Section 3.1 the cross sections for various molecular orientations and the results averaged over all molecular orientations are discussed. The total cross sections calculated within the theoretical models applied in the present work are compared with available theoretical and experimental data in Section 3.2. Concluding remarks are made in Section 4. Atomic units are used throughout the paper.

2 Theory

2.1 The first order Born approximation

Let us consider a process where the projectile ion (P) with $Z_P^{\rm eff}$ effective charge captures an electron form the H_2 molecule. The geometry of the collision system is sketched in Figure 1. At intermediate and high impact velocities (1–2500 keV), that we consider, the collision occurs so quickly that the molecule does not have time to rotate or vibrate appreciably. Therefore, the internuclear vector $\boldsymbol{\rho}$ connecting the two nuclei is taken as constant during the collision [10]. The exact prior version of the transition matrix element for the electron capture is [11]

$$\mathcal{T}_{if}^{\rm prior} = \left\langle \psi_f^- \left| V_i \right| \varphi_i^+ \right\rangle. \tag{1}$$

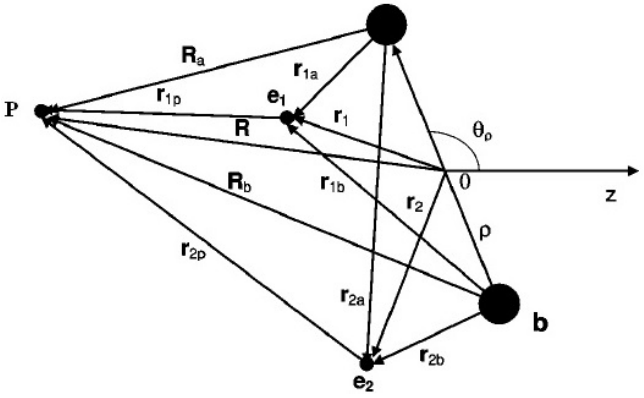

Fig. 1. Scheme of the collision system with the definition of the used coordinates. P denotes the projectile; a, b denote the atoms of the target; e_1, e_2 are the electrons of the target; z is the direction of the beam [11].

Here φ_i^+ is the non-perturbed wave function in the initial channel which is written as

$$\varphi_i^+ = \frac{e^{i\mathbf{K}_i\cdot\mathbf{R}}}{(2\pi)^{3/2}}\phi_i(\boldsymbol{\rho}, \boldsymbol{r}_1, \boldsymbol{r}_2), \tag{2}$$

where $\phi_i(\boldsymbol{\rho}, \boldsymbol{r}_1, \boldsymbol{r}_2)$ is the initial molecular bound state that is given by the following expression [17]

$$\phi_i(\boldsymbol{\rho}, \boldsymbol{r}_1, \boldsymbol{r}_2) = N_{HL}(\rho)\left[e^{-\alpha^* r_{1a}}e^{-\alpha^* r_{2b}} + e^{-\alpha^* r_{1b}}e^{-\alpha^* r_{2a}}\right], \tag{3}$$

with $\alpha^* = 1.166, \rho = 1.406$ and the normalization factor $N_{HL} = \frac{\alpha^{*3}}{\pi^{3/2}}\frac{1}{\sqrt{2(1+s)^2}}$ in which $s = \frac{e^{-\alpha^*\rho}}{3}(\rho^2\alpha^{*2}+3\rho\alpha^*+3)$ and r_{ij} is the relative distance of the ith electron from the nucleus $j \equiv a$ or b. Within the first Born approximation, the final wave function ψ_f^- is expressed by

$$\psi_f^- = \frac{e^{i\mathbf{K}_f\cdot\mathbf{R}}}{(2\pi)^{3/2}}\phi_f(\boldsymbol{\rho}, \boldsymbol{r}_2)\phi_c(\boldsymbol{r}_1), \tag{4}$$

where ϕ_f is the bound state wave function of the residual H_2^+ molecular ion represented by a simple linear combination of atomic orbitals

$$\phi_f(\boldsymbol{\rho}, \boldsymbol{r}_2) = N_f(\rho)(e^{-\alpha r_{2a}} + e^{-\alpha r_{2b}}), \tag{5}$$

with $\alpha = 1.3918$ and the normalization factor $N_f(\rho) = \alpha^{3/2}[(2\pi(1 + \exp(-\alpha\rho) + \alpha\rho + (\alpha\rho)^3/3]^{-1/2}$. Furthermore, in equation (4) $\phi_c(\boldsymbol{r}_1) = \sum_i C_i \exp(-\zeta_{pi} r_1)$ is the Roothaan-Hartree-Fock wave function of the captured electron by the He^+ ion, with C_i expansion coefficients and ζ_{pi} orbital exponents [12]. $\mathbf{K}_i$ and $\mathbf{K}_f$ denote the momentum vectors for the relative motions of the heavy particles in the initial and the final channels, respectively. V_i is the perturbation in the entrance channel given by

$$V_i = \frac{Z_P^{\rm eff} Z_T}{R_a} + \frac{Z_P^{\rm eff} Z_T}{R_b} - \frac{Z_P^{\rm eff}}{r_{1p}} - \frac{Z_P^{\rm eff}}{r_{2p}} \tag{6}$$

with $Z_T = 1$, the charge of the two nuclei in the molecule. We can write the transition matrix (1) as

$$\mathcal{T}_{if}^{\text{prior}} = N(\rho)\Big\langle \phi_c(\boldsymbol{r}_1)(e^{-\alpha r_{2a}} + e^{-\alpha r_{2b}})\,|V_i|\,e^{i\mathbf{K}\cdot\mathbf{R}} \times (e^{-\alpha^* r_{1a}}e^{-\alpha^* r_{2b}} + e^{-\alpha^* r_{1b}}e^{-\alpha^* r_{2a}})\Big\rangle = \sum_{j,l j\neq l} \mathcal{T}_{j,l}^{\text{dir}} + \mathcal{T}_{j,l}^{\text{ind}} \qquad j,l = a,b \tag{7}$$

with $N(\rho) = 2N_f(\rho)N_{HL}(\rho)/(2\pi)^3$ (the factor 2 is because of the two electrons) and $\mathbf{K} = \mathbf{K}_i - \mathbf{K}_f$, where the direct term

$$\mathcal{T}_{j,l}^{\text{dir}} = N(\rho)\Big\langle \phi_c(\boldsymbol{r}_1)(e^{-\alpha r_{2j}} + e^{-\alpha r_{2l}})\left|\frac{Z_P^{\text{eff}}Z_T}{R_j} - \frac{Z_P^{\text{eff}}}{r_{1p}}\right| \times e^{i\mathbf{K}\cdot\mathbf{R}}(e^{-\alpha^* r_{1j}}e^{-\alpha^* r_{2l}})\Big\rangle$$

describes the capture of electron 1 from center $j = a$ or b by means of the interaction of the projectile with this electron situated at center j. The indirect term

$$\mathcal{T}_{j,l}^{\text{indir}} = N(\rho)\Big\langle \phi_c(\boldsymbol{r}_1)(e^{-\alpha r_{2j}} + e^{-\alpha r_{2l}})\left|\frac{Z_P^{\text{eff}}Z_T}{R_l} - \frac{Z_P^{\text{eff}}}{r_{2p}}\right| \times e^{i\mathbf{K}\cdot\mathbf{R}}(e^{-\alpha^* r_{1j}}e^{-\alpha^* r_{2l}})\Big\rangle$$

may be considered as capture of electron 1 from center j through the interaction of the projectile with electron 2 and with the other center labeled l. Of course, the electrons are shared by both nuclei in the molecule and the matrix elements admit this interpretation. However, as in the two-effective center approximation [8], we neglect the indirect term in the present calculations.

After some algebra, $\mathcal{T}_{if}^{\text{prior}}$ can be written in the following compact form

$$\mathcal{T}_{if}^{\text{prior}} = 2N(\rho)\left[\mathcal{L}(\alpha,\alpha^*) + \mathcal{L}(\alpha+\alpha^*,0)\right] \times \left[Z_P^{\text{eff}}Z_T U_{R_a} - Z_P^{\text{eff}}U_{r_{1p}}\right]\cos\left(\frac{-\mathbf{K}\cdot\boldsymbol{\rho}}{2}\right) \tag{8}$$

where $\mathcal{L}$ is a two-center integral given by

$$\mathcal{L}(\alpha,\beta) = \int d\mathbf{r}_2 e^{-\alpha r_{2a}}e^{-\beta r_{2b}} = \frac{8\pi}{C^3\rho}\left[\alpha(\rho C - 4\beta)e^{-\beta\rho} + \beta(\rho C + 4\alpha)e^{-\beta\rho}\right] \tag{9}$$

with $C = \alpha^2 - \beta^2$. U_{R_a} and $U_{r_{1p}}$ are given as below

$$U_{R_a} = \Sigma_i C_i U_i(R_a) = \Sigma_i C_i \int d\mathbf{R}_a d\mathbf{r}_{1a}\frac{e^{i\mathbf{K}\cdot\mathbf{R}_a}}{R_a}e^{-\zeta_{pi}r_{1p}}e^{-\alpha^* r_{1a}} \tag{10}$$

$$U_{r_{1p}} = \Sigma_i C_i U_i(r_{1p}) = \Sigma_i C_i \int d\mathbf{R}_a d\mathbf{r}_{1a}\frac{e^{i\mathbf{K}\cdot\mathbf{R}_a}}{r_{1p}}e^{-\zeta_{pi}r_{1p}}e^{-\alpha^* r_{1a}}. \tag{11}$$

These six-dimensional integrals can be reduced to some one-dimensional integrals. To this end, we consider $U_i(r_{1p})$. Taking the Fourier transform of the term involving r_{1p} according to

$$\frac{e^{-\zeta_{pi}r_{1p}}}{r_{1p}} = -\frac{1}{2\pi^2}\int d\mathbf{q}\frac{e^{i\mathbf{q}\cdot\mathbf{r_{1p}}}}{q^2+\zeta_{pi}^2}.$$

The inner integral can be reduced to their closed forms using the following integral identity

$$\int d\mathbf{r}_{1a}e^{-\alpha^* r_{1a} - i\mathbf{q}\cdot\mathbf{r}_{1a}} = -4\pi\frac{\partial}{\partial\alpha^*}\frac{1}{q^2+\alpha^{*2}}.$$

The result is

$$U_i(r_{1p}) = \frac{2}{\pi}\frac{\partial}{\partial\alpha^*}\int d\mathbf{R}_a e^{i\mathbf{K}\cdot\mathbf{R}_a}\int_0^1 dx \times \int d\mathbf{q}\frac{e^{i\mathbf{q}\cdot\mathbf{R}_a}}{(q^2+\zeta_{pi}^2)(q^2+\alpha^{*2})}. \tag{12}$$

Using the Feynman identity [18] and the integral identity

$$\int d\mathbf{q}\frac{e^{i\mathbf{q}\cdot\mathbf{R}_a}}{[q^2+\Delta_i^2]^2} = \frac{\pi^2}{\Delta_i}e^{-\Delta_i R_a},$$

after some manipulations equation (12) leads to a one-dimensional integral of the following final form

$$U_i(r_{1p}) = 2\pi\frac{\partial}{\partial\alpha^*}\int_0^1 dx\frac{1}{\Delta_i}\frac{\partial}{\partial\Delta_i}\frac{4\pi}{\Delta_i^2+K^2}. \tag{13}$$

An analogous technique leads to a similar expression for $U_i(R_a)$

$$U_i(R_a) = 2\pi\frac{\partial}{\partial\alpha^*}\frac{\partial}{\partial\zeta_{pi}}\int_0^1 dx\frac{1}{\Delta_i}\frac{4\pi}{\Delta_i^2+K^2} \tag{14}$$

with $\Delta_i = \sqrt{\zeta_{pi}^2(1-x) + x\alpha^{*2}}$ and $\alpha^* = 1.166$.

Finally, the cross section differential in scattering angle of the projectile $\Omega \equiv (\theta,\phi)$ for a given molecular orientation $\Omega_\rho \equiv (\theta_\rho,\phi_\rho)$, the doubly differential cross section (DDCS) can be written as

$$\frac{d^2\sigma}{d\Omega d\Omega_\rho} = \frac{\mu_i\mu_f}{2\pi^2}\frac{K_f}{K_i}N(\rho)\left[\mathcal{L}(\alpha,\alpha^*) + \mathcal{L}(\alpha+\alpha^*,0)\right]^2 \times \left|Z_p^{\text{eff}}Z_T U_{R_a} - Z_p^{\text{eff}}U_{r_{1p}}\right|^2 \times 2\pi\left[1 + \frac{\sin(K\rho)}{K\rho}\right] \tag{15}$$

where μ_i and μ_f are the reduced masses before and after the collisions.

2.2 The CTMC approximation

The CTMC method is based on the numerical solution of the classical equations of motion for a large number of trajectories of the interacting particles under randomly

chosen initial conditions [20,36]. In the present work we applied the CTMC model developed recently for molecule targets. Here we give only a brief summary of the model, for details see references [37,39].

Assuming the validity of the independent particle model (IPM), we apply a three-body CTMC approach that considers the interaction between the projectile, an active electron, and the ion core of the molecule. With neglect of relativistic effects, we solve Newton's equations of motion for the three particles:

$$m_i \frac{d^2\mathbf{r}_i}{d\,t^2} = \sum_{j(\neq i)=1}^{3} \mathbf{F}_{ij}(\mathbf{r}_i - \mathbf{r}_j), \quad (i = 1, 2, 3). \tag{16}$$

Here m_i and $\mathbf{r}_i$ are the masses and the position vectors of the three particles, respectively. Using the notations e, P, and T for the electron, projectile, and target, the $\mathbf{F}_{ij}$ forces in (16) are the e-P, e-T, and P-T interactions. The e-T force is determined as $-\nabla_{\mathbf{r}_{ij}} V_{\rm mod}(\mathbf{r}_{ij})$, where $\mathbf{r}_{ij} = \mathbf{r}_i - \mathbf{r}_j$ is the relative position vector of the two particles. $V_{\rm mod}(\mathbf{r})$ is a multi-center *model* potential that describes the interaction of the active electron in the mean field created by the nuclei and the rest electrons of the molecule. For a bare ion projectile of charge $Z_{\rm P}$ the P-T force is derived similarly: $-Z_{\rm P}\nabla_{\mathbf{r}_{ij}}[-V_{\rm mod}(\mathbf{r}_{ij})]$. The e-P interaction in this case is Coulombic. For a structured projectile ion we apply the Green-Sellin-Zachor (GSZ) potential [43] for the determination of the e-P and P-T interactions:

$$V^{\rm GSZ}(r) = -\{Z_{\rm P} - (N_{\rm P} - 1)[1 - \Omega(r)]\}/r, \tag{17}$$

where $Z_{\rm P}$ is the nuclear charge, $N_{\rm P}$ is the number of the electrons in the ion +1, and

$$\Omega(r) = \{(\eta/\xi)\,[\exp(\xi r) - 1] + 1\}^{-1}.$$

The parameters η and ξ depend on $Z_{\rm P}$ and $N_{\rm P}$, their values are tabulated in reference [21]. The e-P force is expressed as $-\nabla_{\mathbf{r}_{ij}} V^{\rm GSZ}(\mathbf{r}_{ij})$. The P-T force is obtained in the same way as for the bare ion projectile but with use of an *effective* ion charge $Z_{\rm P}^{\rm eff}$. The latter is determined from the GSZ potential: $Z_{\rm P}^{\rm eff} = -rV^{\rm GSZ}(r)$.

The molecular potential $V_{\rm mod}(\mathbf{r})$ is approximated by the sum of screened atomic potentials. For the hydrogen molecule considered in this work:

$$V_{\rm mod}(\mathbf{r}) = V_{\rm H}(r_{\rm H1}) + V_{\rm H}(r_{\rm H2}). \tag{18}$$

Here $r_{{\rm H}i} = |\mathbf{r} - \mathbf{r}_{{\rm H}i}|$ is the distance of the electron from the nucleus of the ith hydrogen atom located at $\mathbf{r}_{{\rm H}i}$. $V_{\rm H}(r_{{\rm H}i})$ is approximated by the GSZ potential:

$$V_{\rm H}(r_{{\rm H}i}) \approx V^{\rm GSZ}(r_{{\rm H}i}) = -\{Z_{\rm H} - (N_{\rm H} - \Delta N_{\rm H} - 1) \times [1 - \Omega(r_{\rm H})]\}/r_{{\rm H}i}. \tag{19}$$

Comparing the form of the above expression with that of equation (17), one sees that the GSZ potential is modified by introducing the change of the electron number at the atomic centers, $\Delta N_{\rm H}$. This can be justified considering that the potentials at the atomic centers differ from those of the isolated atoms. For the parametrization of the potential (19) we may start from the approximate picture of the hydrogen molecule as consisting of two neutral hydrogen atoms. The potential for the (e + H°) system is obtained by $Z_{\rm H} = 1$ and $N_{\rm H} = 2$. With this choice the value of $\Delta N_{\rm H}$ is determined by the condition of the asymptotical dependence of the molecular potential

$$V_{\rm mod}(\mathbf{r})(r \to \infty) = -\frac{1}{r} \tag{20}$$

that gives $\Delta N_{\rm H} = 0.5$. We note that at each H atomic centers in the limit $r_{{\rm H}i} \to 0$ equation (19) leads to the potential

$$V_{\rm A}(r_{{\rm H}i}) = -\frac{1}{r_{{\rm H}i}}. \tag{21}$$

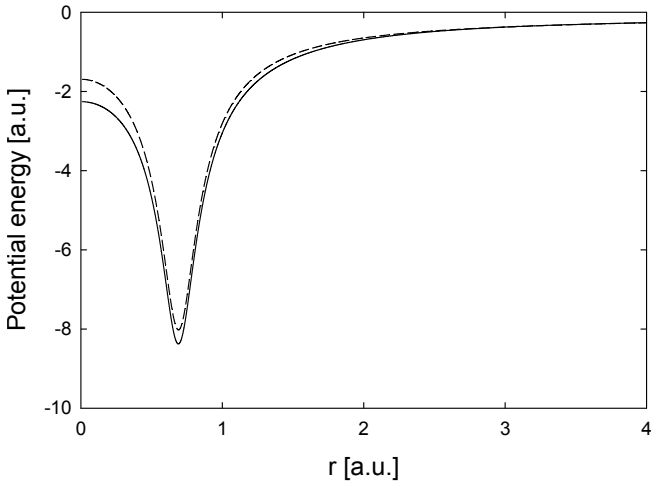

Fig. 2. The potential energy of the electron in the hydrogen molecule at an angle of 80° relative to the axis of the molecule. Solid curve, present model potential; dashed curve, the model potential proposed by Meng et al. [38].

In Figure 2 we plotted the potential energy of the electron in the hydrogen molecule given by equation (19). The distance r is measured from the center of the molecule, and the electron is located in a direction of 80° relative to the axis of the molecule. We used $\eta = 0.6298$ and $\xi = 1.325$ in the $\Omega(r)$ function [21]. Also presented in the figure is the potential used by Meng et al. [38] in their four-body CTMC model. The four particles of the latter model are the projectile, the two electrons and the target nuclei located at a constant distance of 1.402 a.u. from each other. Meng et al. considered the collisions of fully stripped ions with H_2. They exactly took account all the interactions between the four particles, except that the electron-electron interaction was approximated by a mean potential. The two-center molecular potential of Meng et al. reads

$$V_{\rm mod}(\mathbf{r}) = -\frac{1}{r_{\rm H1}} - \frac{1}{r_{\rm H2}} + \frac{1}{r}\left[1 - (1 + \lambda r)\exp(-2\lambda r)\right], \tag{22}$$

where $\lambda = 1.166$. As is seen from Figure 2, the potential proposed in the present work is close to that expressed by the above equation.

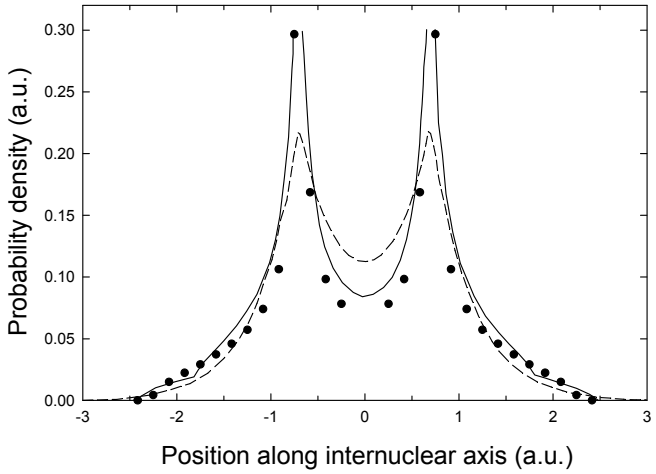

Fig. 3. The initial probability density of the electron in the hydrogen molecule along the internuclear axis. The closed circles and the solid line denote the result of the present CTMC procedure and that of the four-body CTMC model of Meng et al. [38], respectively. The dashed line represents the quantum-mechanical distribution calculated by Wang [40].

For the random choice of the initial values of the position and momentum coordinates of the electron the method of Reinhold and Falcón [19] was generalized to the case of the anisotropic molecular potential. Details of the procedure can be found in references [37,39]. The random choice of the angular variables is the same as in the standard CTMC theory. For the random choice of the radial distance r a generalized version of equation (11) in reference [19] is used:

$$\omega(r,\theta_r,\phi_r) = \int_0^r dr' \mu\, r'^2 \left\{2\mu[E_i - V_{\rm mod}(r',\theta_r,\phi_r)]\right\}^{1/2}, \tag{23}$$

where μ and E_i are the reduced mass and binding energy of the electron, respectively, and the position vector the electron is expressed by the polar coordinates, $\mathbf{r} = (r,\theta_r,\phi_r)$. The range of the radial distance in the direction (θ_r,ϕ_r) is confined to the interval $0 < r < r_0(\theta_r,\phi_r)$ because of the condition that the kinetic energy is positive. The maximum value $r_0(\theta_r,\phi_r)$ is obtained as the root of the equation

$$E_i - V_{\rm mod}(r,\theta_r,\phi_r) = 0. \tag{24}$$

The determination of r starts with the random choice of an ω value in the interval $[0,\omega(r_0)]$ in a selected direction (θ_r,ϕ_r). Then r is obtained from the inverse of the $\omega(r,\theta_r,\phi_r)$ function given by equation (23). A further ingredient of the procedure is the so-called "volume correction" by which the choice of the different directions in the molecule is weighted. The weight function is determined assuming that the probability of finding an electron at a given (θ_r,ϕ_r) direction is proportional to the volume of the integration in equation (23) at the maximum radial distance, $\Delta V \propto r_0^3(\theta_r,\phi_r)$.

As a check of the above procedure, in Figure 3 we compared the initial probability density of the electron along the internuclear axis of H_2 with that obtained by Meng et al. [38] in their four-body CTMC model. The figure shows also the quantum-mechanical result for the ground state of the molecule as calculated by Wang [40]. The agreement between the two CTMC models is good.

Besides the position and momentum coordinates of the electron, a further initial characteristics of the molecule is its orientation. In experiments that determine integrated (total) cross sections no information exists about the orientation of the molecule. Accordingly, in the calculations we also assume a random orientation. This is implemented in the present CTMC model by the random rotation of the molecule using the three Euler angles at each collision event.

Further details of the calculations are as follows. Assuming the validity of the Franck-Condon approximation, the calculations were carried out at fixed, equilibrium geometry of the H_2 molecule. We used the value 1.4 a.u. for the ground-state internuclear distance, and 0.567 a.u. for the ground-state binding energy.

The integration of the equations of motion was started at such a large distance R_0 between the incoming projectile and the molecule at which the relative change of the binding energy of the electron due to the perturbation by the projectile was less than 10^{-4}. After the collision the calculations were made in two steps. In the first step the integration was continued until the projectile recedes to the same distance as that of the initial approach, R_0. This distance is large enough to identify the main reaction channels (excitation, ionization, and charge transfer). In the second step only collision events leading to ionization are regarded, and the trajectories of the particles are calculated up to $R = 10^3$ a.u.

The goal of the present CTMC calculations was the determination of the cross section for the process of the single electron capture. By the analysis of the calculated electron trajectories one-electron ionization and capture probabilities can be deduced as a function of the impact parameter b. Introducing the notation $p_c(b)$ for the capture probability, in the independent particle model the probability of the event that only one electron is captured is given by

$$P(b) = 2\,p_c(b)\,[1 - p_c(b)]\,. \tag{25}$$

The cross section is obtained as

$$\sigma = 2\pi \int_0^\infty b\,P(b)\,db. \tag{26}$$

As a further check of the present CTMC model, in Figure 4 we compared the results of our calculations for the single electron capture from the H_2 molecule by *bare* He^{2+} ion with those obtained by Meng et al. [38] in their four-body CTMC model. Also plotted in the figure are the experimental data measured by Shah and Gilbody [41] and Hvelplund and Andersen [25]. The agreement between the two CTMC models is excellent. Both theories provide a good description of the experimental data except below 10 keV amu^{-1}, where the present calculations show an increasing deviation from the experiment with decreasing impact energy.

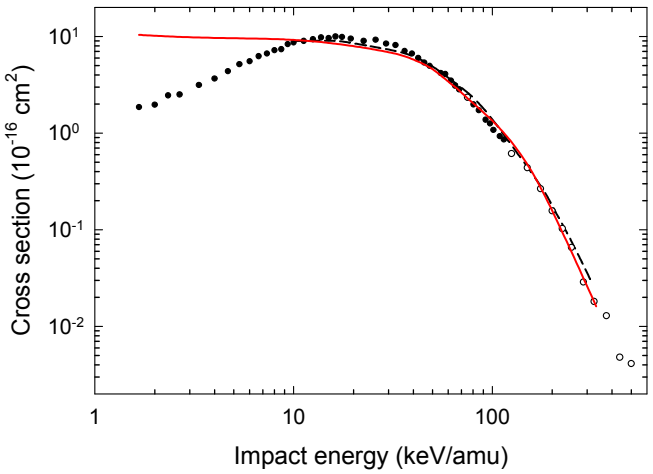

Fig. 4. Single electron capture cross section for He^{2+} on H_2 collisions. Theories: solid line, present CTMC; dashed line, four-body CTMC of Meng et al. [38]. Experimental data: closed circles, Shah and Gilbody [41]; open circles, Hvelplund and Andersen [25].

2.3 The quasi-molecular description

The molecular model applied in the present work has been discussed in details in previous works [26–29], here we give only a short summary. The main approximations of the model are as follows. It is a semi-classical (impact-parameter) description: the motion of the nuclei is determined by the classical mechanics, while the dynamics of the electrons is treated quantum mechanically. The projectile ion is assumed to follow a straight-line trajectory, $\mathbf{R}(t) = \mathbf{b} + \mathbf{v}t$. Here $\mathbf{R}$ is the distance between the He^+ ion and the center of mass of the H_2 molecule, and $\mathbf{v}$ is the collision velocity.

The model applies the sudden approximation for the roto-vibrational motion of the molecules, considering that the electronic transitions are much faster than the rotation and vibration motions. Furthermore, due to the regarded relatively large collision velocities, it is assumed that the roto-vibrational wavefunction of H_2 does not change appreciably during the collision, and, therefore, the calculations can be performed with a frozen (ground-state) internuclear distance ρ, and with a constant molecular orientation angle θ.

The evolution of the electronic wave function of the collision system is governed by the time-dependent Schrödinger equation

$$\hat{H}_{\rm el}\,\psi(\mathbf{r};\boldsymbol{\rho},\mathbf{b},\mathbf{v},t) = -i\frac{\partial}{\partial t}\psi(\mathbf{r};\boldsymbol{\rho},\mathbf{b},\mathbf{v},t). \qquad (27)$$

Here $\mathbf{b}$, $\mathbf{v}$ and $\boldsymbol{\rho}$ are constant parameters in $\psi(\mathbf{r};\boldsymbol{\rho},\mathbf{b},\mathbf{v},t)$. $\hat{H}_{\rm el}$ is the clamped-nuclei Born-Oppenheimer electronic Hamilton operator. To find the solution of equation (27), ψ is expanded on the basis of the eigenfunctions $\{\varphi_i\}$ and eigenvalues $\{\epsilon_i\}$ of $\hat{H}_{\rm el}$:

$$\psi(\mathbf{r};\boldsymbol{\rho},\mathbf{b},\mathbf{v},t) = \sum_j a_j(\boldsymbol{\rho},\mathbf{b},\mathbf{v},t)\,\varphi_j(\mathbf{r};\boldsymbol{\rho},\mathbf{R}(t)) \times \exp\left[-i\int_0^t \epsilon_j(\boldsymbol{\rho},\mathbf{R}(t'))\,dt'\right] \qquad (28)$$

with

$$\hat{H}_{\rm el}\,\varphi_j(\mathbf{r};\boldsymbol{\rho},\mathbf{R}) = \epsilon_j(\boldsymbol{\rho},\mathbf{R})\,\varphi_j(\mathbf{r};\boldsymbol{\rho},\mathbf{R}). \qquad (29)$$

Replacing the expansion (28) into equation (27), one obtains the following system of coupled differential equations:

$$i\frac{da_j(t)}{dt} = \sum_k a_k(t)\left\langle \varphi_j\left|\hat{H}_{\rm el} - i\frac{\partial}{\partial t}\right|\varphi_k\right\rangle \times \exp\left[-i\int_0^t (\epsilon_k - \epsilon_j)\,dt'\right]. \qquad (30)$$

The decomposition of the matrix elements $\langle\varphi_j|\frac{\partial}{\partial t}|\varphi_k\rangle$ containing the dynamical (non-adiabatic) couplings into those containing the radial and rotational couplings, $\langle\varphi_j|\frac{\partial}{\partial R}|\varphi_k\rangle$ and $\langle\varphi_j|iL_y|\varphi_k\rangle$ respectively, leads to

$$i\frac{da_j(t)}{dt} = \sum_k a_k(t)\left(\langle\varphi_j|\hat{H}_{\rm el}|\varphi_k\rangle - i\frac{vR_z}{R}\left\langle\varphi_j\left|\frac{\partial}{\partial R}\right|\varphi_k\right\rangle - i\frac{vb}{R^2}\langle\varphi_j|iL_y|\varphi_k\rangle\right) \times \exp\left[-i\int_0^t (\epsilon_k - \epsilon_j)\,dt'\right]. \qquad (31)$$

In solving the coupled differential equations we considered number of states of the HeH_2^+ quasi-molecule which could be correlated with the entry channel and result in charge-exchange by means of non-adiabatic couplings. In the choice of the states we assumed that the electron spin was conserved in the collision. The potential energy curves and the non-adiabatic coupling matrix elements [30] between the relevant states were computed as functions of R, whereas ρ was kept fixed at its optimized value in the ground state. The molecule structure calculations were made by the quantum chemistry software package MOLPRO [31]. We applied the state-averaged Complete Active Space Self-Consistent Field method to carry out computations for the lowest five electronic states of the HeH_2^+ quasi-molecule with equal weight factors:

$He(1\,^1S) + H_2^+(X\,^2\Sigma_g^+)$
$He^+(1\,^2S) + H_2(X\,^1\Sigma_g^+)$ (entry channel)
$He(1\,^3S) + H_2^+(X\,^2\Sigma_g^+)$
$He(2\,^1S) + H_2^+(X\,^2\Sigma_g^+)$
$He(1\,^3P) + H_2^+(X\,^2\Sigma_g^+)$.

After solving the coupled equations the probability and the partial cross section of a capture channel f is obtained as

$$P_f(b,v;\rho,\theta) = \lim_{t\to+\infty} |a_f(t;\rho,\theta,b,v)|^2, \qquad (32)$$

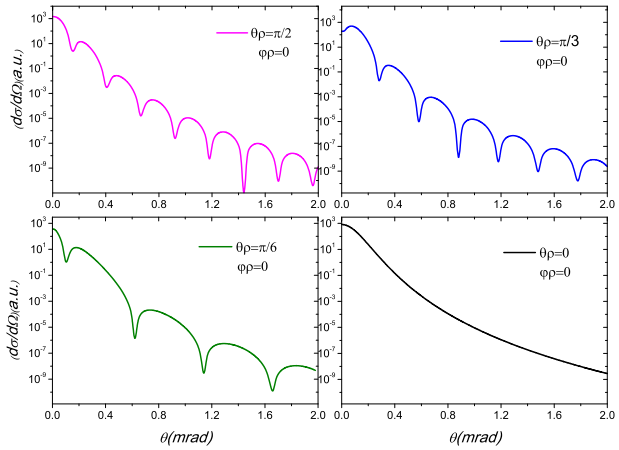

Fig. 5. DDCS for single electron capture from hydrogen molecule by He^+ ion at 1 MeV amu^{-1} incident energy for various molecular orientations: $\theta_\rho = 0; \pi/6; \pi/4; \pi/3; \pi/2$ rad and $\phi_\rho = 0$.

and

$$\sigma_f(v, \rho, \theta) = 2\pi \int_0^\infty P_f(b, v; \rho, \theta) b\, db, \qquad (33)$$

respectively.

The partial cross sections for the transitions between the different quasi-molecular states involved in the charge transfer process were calculated numerically using the EIKONXS code based on an efficient propagation method [32]. The total cross section was then obtained with summation over all charge exchange channels and by averaging for nine different molecular orientations. The orientation averaged cross section was approximated by the Franck-Condon formula for homo-nuclear targets [33]. The calculations were made in the 1–200 keV laboratory energy range (0.17–2.45 a.u. collision velocities).

3 Results and discussion

3.1 Differential cross sections

In this subsection the results for various differential cross sections for the $He^+ + H_2$ collision evaluated in the B1 model are discussed. At present there are no experimental data for the capture from oriented hydrogen molecules, therefore, only the theoretical results are discussed.

In Figure 5 DDCSs (see Eq. (15)) at incident energy 1 MeV for fixed molecular orientations are presented. The oscillating behavior of the DDCS as a function of θ is well visible in the figure. The interference patterns are attributed to the term $\cos(-\frac{\mathbf{K}\boldsymbol{\rho}}{2})$ in the transition amplitude (8) or to the term $\sin(K\rho)$ in the differential cross section (15). Both the two-body interaction potentials $V_{\rm PT}$ and $V_{\rm Te}$ contribute to the interference structure. As it can be seen from this figure, for $\theta_\rho = 0$, i.e. when the target axis is parallel to the incident beam direction, there is no interference pattern. The same happens when $\theta_\rho = \pi$. As θ_ρ increases or decreases from the parallel direction to larger or lower angles, the interference pattern becomes more visible and the number of oscillations in a fixed angular range of the scattering angle θ increases. Obviously, the diffraction pattern is the most dominant when the direction of the molecular axis is perpendicular to the incident beam direction. The observed interference pattern shows similarity with that appearing in Young's double-slit experiment. The two atomic centers of the target play the role of the double slit in this case.

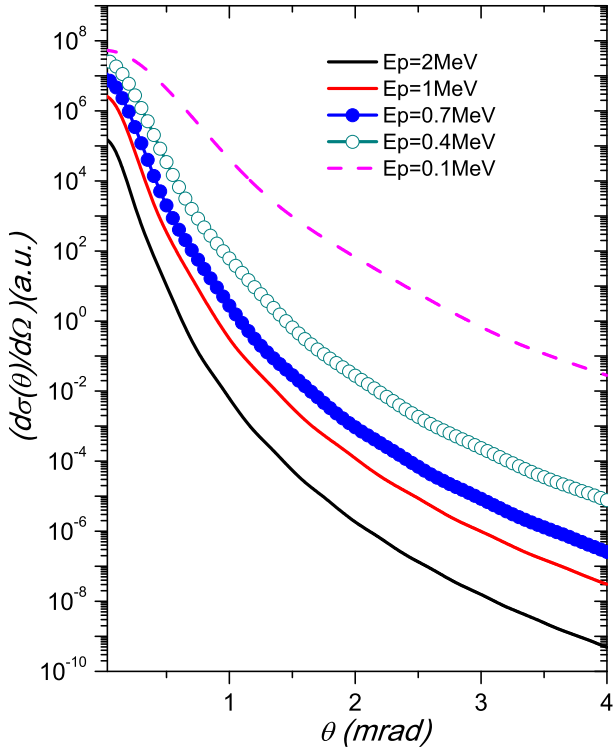

Fig. 6. Single differential cross sections (see Eq. (34)) for the $He^+ + H_2 \rightarrow He^\circ + H_2^+$ collisions at various impact energies.

The interference pattern depends upon the distance between the slits $d = \rho \sin\theta_\rho$ and the wavelength of the scattered particle (λ). For a definite value of wavelength and a definite range of the scattering angle ($0 < \theta < \theta_{\rm max}$) the maximum number of oscillations is $m = \frac{2\rho \sin\theta_\rho \sin\theta_{\rm max}}{\lambda}$. As the scattering angle θ increases, the number of oscillations increases and its maximum occurs at $\theta_\rho = \pi/2$ rad [23].

Figure 6 presents single differential cross sections for various projectile energies obtained by averaging the DDCS (15) over all directions of the molecular axes ρ,

$$\frac{d\sigma}{d\Omega} = \frac{1}{4\pi} \int \frac{d^2\sigma}{d\Omega d\Omega_\rho} d\Omega_\rho. \qquad (34)$$

In all the curves, the oscillating structure observed for the DDCS in Figure 5 disappeared completely. It can be seen from Figure 6 that the single differential cross section decreases monotonously with the increase of θ for all impact energies. Interestingly, there is no indication of the Thomas two-step scattering mechanism even at the highest impact energy [23].

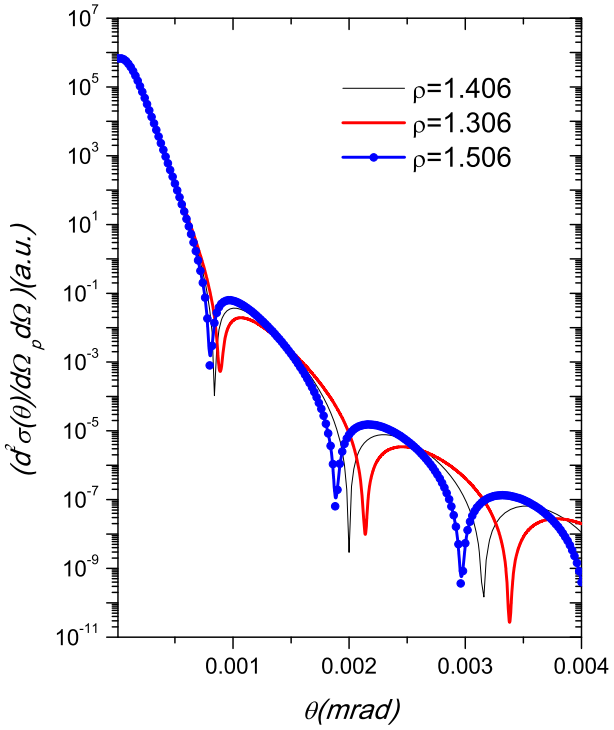

Fig. 7. Dependence of the interference patterns in the DDCS on the internuclear separation at 1.3 MeV impact energy. The direction of the molecule is: $\theta_\rho = \pi/2$ and $\phi_\rho = 0$ rad.

In Figure 7 DDCSs evaluated for different internuclear distances are presented. The impact energy is 1.0 MeV and the direction of the molecule is fixed for $\theta_\rho = \frac{\pi}{2}, \phi_\rho = 0$ and three various internuclear separations, $\rho = 1.306, 1.406$ and 1.506 are considered. It is well seen that the variation of internuclear distance causes displacements of the peaks in the angular distribution of the double differential cross section.

Figure 8 presents the

$$\frac{d\sigma}{d\cos\theta_\rho} = \frac{1}{2\pi}\int_0^{2\pi} d\phi_\rho \int \frac{d^2\sigma}{d\Omega d\Omega_\rho} d\Omega \qquad (35)$$

single differential cross section as a function of θ_ρ at 1.0 MeV impact energy for three different values of nuclear separation. The three curves have a similar shape but the magnitude of the cross sections depends on the value of ρ especially at the two end angles, $\theta_\rho = 0$ and $\theta_\rho = 180°$.

DDCSs for fixed, perpendicular molecular orientation with respect to the incident beam ($\theta_\rho = \pi/2$ and $\phi_\rho = 0$) at various projectile energies are shown in Figure 9. We know that by increasing the projectile energy, the wavelength of the incoming particle decreases, so the number of peaks in a definite θ interval increases. The number of peaks in the 2 mrad angular interval are 3 and 5 for 400 keV and 1.5 MeV impact energies, respectively. It can also be seen from the figure that as the projectile energy increases the differential cross section decreases rapidly.

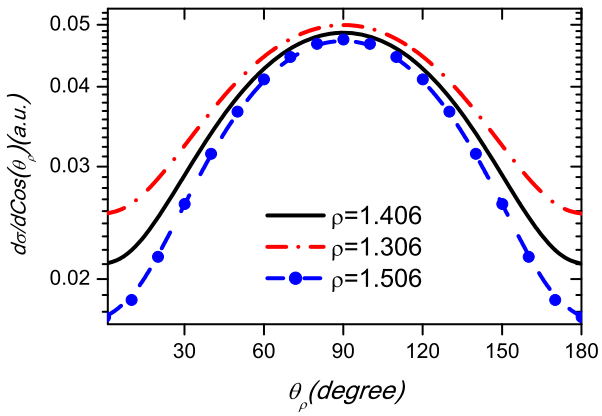

Fig. 8. $d\sigma/d\cos\theta_\rho$ versus θ_ρ at different internuclear separations for 1.0 MeV impact energy.

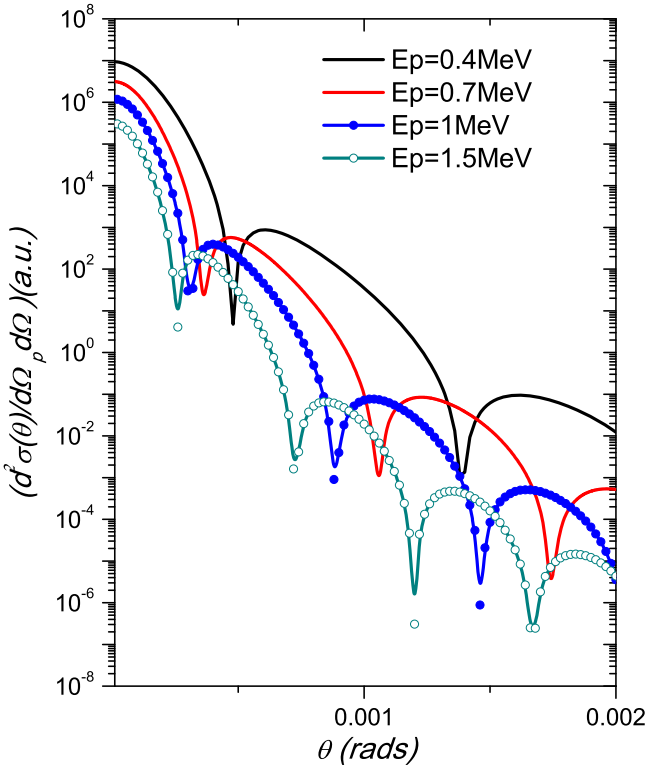

Fig. 9. Double differential cross sections for fixed orientations of the molecular axis (ρ is perpendicular to the incident beam) at different projectile energies.

3.2 Total cross sections

The total cross section (TCS) integrated over projectile scattering angle and averaged over all possible orientations of the molecule is given by

$$\sigma = \frac{1}{4\pi}\int d\Omega_\rho \int d\Omega \frac{d^2\sigma}{d\Omega d\Omega_\rho}. \qquad (36)$$

In Figure 10, TCS's calculated in B1 for the single-electron capture from H_2 molecule by the impact of 1–5000 keV

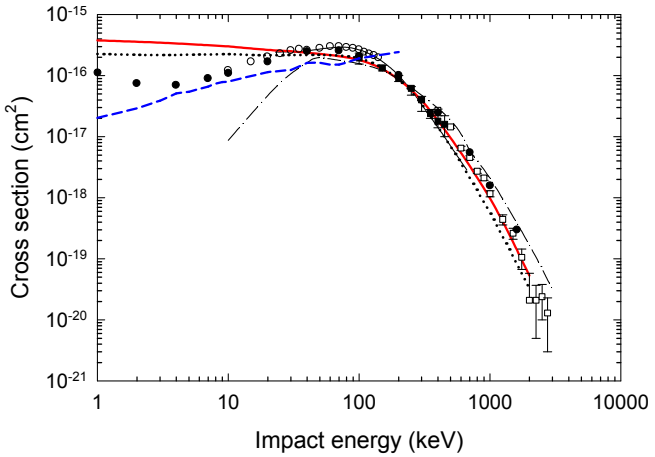

Fig. 10. Total cross section for single electron capture in He^+ on H_2 collisions. Theories: thick solid line (red), present CTMC; thin solid line, five-body CTMC of Alessi et al. [22]; dotted line, present atomic CTMC; dashed-dotted line, present B1; thick dashed line (blue), present quasi-molecular model. Experimental data: closed circles, Oak Ridge National Laboratory (ORNL) data tables [35]; closed squares, Allison et al. [24]; open circles, de Heer et al. [34]; open squares, Hvelplund and Andersen [25].

He^+ projectiles are compared with several sets of experimental measurements [22,25,34,35] and with other theories. As can be seen, B1 shows a reasonable agreement with the measurements from medium to high impact energy regimes.

In the figure the predictions of the present CTMC theory and the quasi-molecular model (see Sects. 2.2 and 2.3, respectively), as well as the CTMC results of Alessi et al. [22] are also plotted. The CTMC model applied by the latter authors is a five-body description proposed originally by Wood and Olson [42] for the double electron removal from H_2 by collisions with highly charged ions. This model differs from the four-body description of Meng et al. [38] in that the initial state of the molecule is approximated by two independent hydrogen atoms. Each electron is bound initially to its parent atomic center by the Coulomb force, and has no dependence on the other atomic center or the other electron. The internuclear distance is not constant, the interaction between the hydrogen atoms is described by a Morse potential. The electron-electron and electron-nucleus interactions are turned on in the course of the collision when an electron reaches the continuum with respect to its parent nucleus.

Similarly to the present CTMC description, Alessi et al. [22] also used the GSZ potential to represent the interaction of the electrons with the partially stripped He^+ projectile. Besides the total cross section, the authors determined also partial cross sections as a function of the principal quantum number n of the final state of the captured electron. Considering the partially filled ground state of He^+, the cross section for $n = 1$ was reduced by a factor of 1/2. In our CTMC calculations we did not determine n-dependent cross sections. For a consistent comparison between the two models, we estimated the effect of the above factor on the present results. Assuming the $1/n^3$ dependence of the capture cross section, we took into account the effect by applying a correction factor $(0.5 + 1/8 + 1/27 + 1/64 + \cdots)/(1 + 1/8 + 1/27 + 1/64 + \cdots) = 0.578$ to the total cross section.

As it is seen from Figure 10, the two CTMC models are in a reasonable agreement. Both theories provide a good description of the experimental data, except for the range of the low impact energies (below 10 eV) where deviations up to a factor of five occur between the experiment and the present CTMC model.

To see the effect of using the two-center potential in the present CTMC model, we also plotted in Figure 10, the results of an "atomic" CTMC calculation. As an atomic approximation, the cross section for H_2 is calculated simply by taking twice the cross section obtained for the hydrogen atom. For the calculation of the latter we applied the standard CTMC model, in which we used the molecular binding energy ($E_b = -0.567$ a.u.) and an effective target nuclear charge obtained as $Z_T = \sqrt{2|E_b|} = 1.065$. One may conclude from the figure that the difference between the molecular and the atomic approximation is relatively small. In the intermediate energy range the two models resulted in identical cross sections. Larger deviations, up to 70%, occur at the lower lower and higher impact energies.

It was the failure of B1 and CTMC at low collision energies that motivated us to make the quasi-molecular calculations. As is seen in Figure 10, the results of the latter calculations are in a reasonable agreement with the experiment and CTMC at intermediate impact energies. In contrast to CTMC, the quasi-molecular model correctly reproduces the decreasing tendency of the experimental data with decreasing impact energy. However, it does not show the minimum seen in the experimental data at about 4 keV, and below the minimum it strongly underestimates the measured cross sections. The possible reason of this behavior is that we could involve only a few of the densely packed electronic states of the HeH_2^+ in the electronic structure calculations. The involvement of more states would have increased the computation time enormously.

4 Summary and conclusions

The four-body first Born approximation has been applied for the description of the single electron capture by He^+ ions from the hydrogen molecule. Double differential cross sections have been calculated for different orientations of the molecule. The obtained DDCSs show the interference patterns due to the coherent scattering of the particles from the two atomic centers of the molecule. The interference patterns disappeared when the DDCSs were averaged over the orientations of the molecule.

Total cross sections have been obtained by integrating the DDCS over the scattering angle of the projectile and averaging it over the molecular directions. A three-body CTMC model worked out for molecular targets has also been applied for the calculation of total cross sections.

A good agreement has been found between the present CTMC results and the calculations of Alessi et al. [22] made in a more realistic, five-body CTMC approach. To account for the increasing role of the quantum mechanical effects at low impact energies, we made total cross section calculations within a quasi-molecular model.

In lack of differential experimental data for the investigated process, a comparison with the experiment was made only for the total cross section. An acceptable agreement between the present theoretical results and the available experimental data was found only in the intermediate and high-energy regimes of the impact energy. The failure of the B1 approximation below 40 keV is explained by its limited validity. The CTMC and the quasi-molecular model proved to be better descriptions at low energies, but they only partially accounted for the discrepancy between the theory and experiment.

This work was supported by the National Scientific Research Foundation (OTKA, Hungary, Grant No. K109440) and the National Information Infrastructure Program (NIIF, Hungary). Among the authors H.G. acknowledges the support from the Institute for Nuclear Research of the Hungarian Academy of Sciences, and S.D. acknowledges the support from the International Visegrad Fund (Grant No. 51600934).

Author contribution statement

H. Ghavaminia performed Born approximation calculation under the supervision of L. Gulyás. L. Sarkadi performed CTMC calculations. E. Bene and S. Demes carried out the quasi-molecular calculations, Z. Juhász participated in program development. All authors contributed to data interpretation as well as the writing and the revising of the text.

References

1. Dž. Belkić, *Principles of Quantum Scattering Theory* (Institute of Physics Publishing, Bristol and Philadelphia, 2004)
2. N. Stolterfoht, B. Sulik, V. Hoffmann, B. Skogvall, J.Y. Chesnel, J. Rangama, F. Fremont, D. Hennecart, A. Cassimi, X. Husson, A.L. Landers, J.A. Tanis, M.E. Galassi, R.D. Rivarola, Phys. Rev. Lett. **87**, 023201 (2001)
3. S. Dey, I.E. McCarthy, P.J.O. Teubner, E. Weigold, Phys. Rev. Lett. **34**, 782 (1975)
4. I.E. McCarthy, J. Phys. B **6**, 2358 (1973)
5. R.W. Zurales, R.R. Lucchese, Phys. Rev. A **35**, 2852 (1987)
6. R.W. Zurales, R.R. Lucchese, Phys. Rev. A **37**, 1176 (1988)
7. R.D. DuBois, M.E. Rudd, Phys. Rev. A **17**, 843 (1978)
8. P. Weck, O.A. Fojoń, J. Hanssen, B. Joulakian, R.D. Rivarola, Phys. Rev. A **63**, 042709 (2001)
9. P. Weck, O.A. Fojón, B. Joulakian, C.R. Stia, J. Hanssen, R.D. Rivarola, Phys. Rev. A **66**, 012711 (2002)
10. S. Alston, T. Brennant, F. Bannon, Phys. Rev. A **52**, 3899 (1995)
11. C.R. Stia, O.A. Fojón, P.F. Weck, J. Hanssen, B. Joulakian, R.D. Rivarola, Phys. Rev. A **66**, 052709 (2002)
12. E. Clementi, C. Roetti, At. Data Nucl. Data Tables **14**, 177 (1974)
13. H.F. Busnengo, S.E. Corchs, R.D. Rivarola, Phys. Rev. A **57**, 2701 (1998)
14. E. Ghanbari Adivi, J. Phys. B: At. Mol. Opt. Phys. **42**, 095207 (2009)
15. J.M. Monti, R.D. Rivarola, P.D. Fainstein, J. Phys. B: At. Mol. Opt. Phys. **44**, 195206 (2011)
16. D. Fregenal, J.M. Monti, J. Fiol., P.D. Fainstein, R.D. Rivarola, G. Bernardi, S. Surez, J. Phys. B: At. Mol. Opt. Phys. **47**, 155204 (2014)
17. S.C. Wang, Phys. Rev. **39**, 579 (1928)
18. R.P. Feynman, Phys. Rev. **76**, 769 (1949)
19. C.O. Reinhold, C.A. Falcón, Phys. Rev. A **33**, 3859 (1986)
20. R. Abrines, I.C. Percival, Proc. Phys. Soc. Lond. **88**, 861 (1966)
21. R.H. Garvey, C.H. Jackman, A.E.S. Green, Phys. Rev. A **12**, 1144 (1975)
22. M. Alessi, N.D. Cariatore, P. Focke, S. Otranto, Phys. Rev. A **85**, 042704 (2012)
23. E. Ghanbari Adivi, J. Phys. B: At. Mol. Opt. Phys. **43**, 065202 (2010)
24. S.K. Allison, J. Cuevas, P.G. Murphy, Phys. Rev. **102**, 1041 (1956)
25. P. Hvelplund, A. Andersen, Phys. Scr. **26**, 375 (1982)
26. E. Bene, P. Martínez, G.J. Halász, A. Vibók, M.-C. Bacchus-Montabonel, Phys. Rev. A **80**, 012711 (2009)
27. E. Rozsályi, E. Bene, G.J. Halász, Á. Vibók, M.-C. Bacchus-Montabonel, Phys. Rev. A **81**, 062711 (2010)
28. E. Rozsályi, E. Bene, G.J. Halász, Á. Vibók, M.-C. Bacchus-Montabonel, Phys. Rev. A **83**, 052713 (2011)
29. E. Bene, M.-C. Bacchus-Montabonel, Eur. Phys. J. D **68**, 167 (2014)
30. M. Baer, *Beyond Born-Oppenheimer: Electronic Non-Adiabatic Coupling Terms and Conical Intersections* (Wiley, Hoboken, NJ, 2006)
31. MOLPRO package of ab initio programs designed by H.J. Werner, P. Knowles, version 2010.1. See http://www.molpro.net
32. R.J. Allan, C. Courbin, P. Salas, P. Wahnon, J. Phys. B **23**, L461 (1990)
33. E. Rozsályi, L.F. Errea, L. Méndez, I. Rabadán, Phys. Rev. A **85**, 042701 (2012)
34. F.J. de Heer, J. Schutten, H. Moustafa, Physica (Amsterdam) **32**, 1973 (1966)
35. C.F. Barnett, J.A. Ray, E. Ricci, M.I. Wilker, in *Atomic Data for Controlled Fusion Researchn*, ORNL Report No. 5206, Oak Ridge National Laboratory, edited by E.W. McDaniel, E.W. Thomas (Georgia Institute of Technology and H.B. Gilbody, Queens University, Belfast, 1977), Vol. 1
36. R.E. Olson, A. Salop, Phys. Rev. A **16**, 531 (1977)
37. L. Sarkadi, Phys. Rev. A **92**, 062704 (2015)
38. L. Meng, C.O. Reinhold, R.E. Olson, Phys. Rev. A **40**, 3637 (1989)
39. S.T.S. Kovács, P. Herczku, Z. Juhász, L. Sarkadi, L. Gulyás, B. Sulik, Phys. Rev. A **94**, 012704 (2016)
40. S.C. Wang, Phys. Rev. A **31**, 579 (1982)
41. M.B. Shah, H.B. Gilbody, J. Phys. B **11**, 121 (1978)
42. C.J. Wood, R.E. Olson, Phys. Rev. A **59**, 1317 (1999)
43. A.E.S. Green, D.L. Sellin, A.S. Zachor, Phys. Rev. **184**, 1 (1969)